PAPER

Check for updates

Fluorogenic selective detection of Zn^{2+} using a pyrazole-*ortho*-vanillin conjugate: insights from DFT, molecular docking, bioimaging and anticancer applications†

Malavika S. Kumar,[a] Sourav Pakrashy,[b] Sounik Manna,[c] Sujata Maiti Choudhury,[c] Bhriguram Das, [iD][d] Abhishek Ghosh,[e] Asiful H. Seikh,[f] Malay Dolai [iD] *[b] and Avijit Kumar Das [iD] *[a]

A fluorescent sensor, (E)-N'-(2-hydroxy-3-methoxybenzylidene)-3,5-dimethyl-1H-pyrazole-1-carbohydrazide (**HMPC**), was designed and synthesized for the selective fluorescence recognition of Zn^{2+} in semi-aqueous media. Notably, **HMPC** exhibited a red-shifted, two-fold fluorescence "turn-on" enhancement in response to Zn^{2+} at 490 nm, with a detection limit of 1.68 μM, which is significantly lower than the WHO guideline (76.0 μM). The binding constant of **HMPC** with Zn^{2+} was calculated to be 5×10^4 M^{-1}. The fluorescence enhancement of **HMPC** in the presence of Zn^{2+} is attributed to the suppression of the PET process and the enhancement of ICT, leading to fluorescence *via* the CHEF mechanism. The sensing mechanism was demonstrated through UV-vis, fluorescence spectroscopy, Job plots, ESI-MS, and DFT calculations. For biological applications, cytotoxicity and cell imaging studies were performed using MCF-7 cells. Molecular docking studies revealed a high binding energy of **HMPC** ($\Delta G = -7.1$ kcal mol^{-1}) with the 4,5-diaryl isoxazole HSP90 chaperone protein, suggesting its potential as an anticancer agent. Additionally, its binding energy of -6.5 kcal mol^{-1} with the HDAC8 protein indicates greater efficacy than suberoylanilide hydroxamic acid (SAHA) in inhibiting HDAC, as it binds more strongly to the HDAC8 protein than SAHA (-7.4 kcal mol^{-1}). Furthermore, due to its favorable ADME profile, **HMPC** may be suitable for oral administration, enhancing its potential as an anticancer drug.

1. Introduction

A chemosensor is an abiotic molecule that produces a measurable signal when interacting with matter or energy. Fluorescent chemosensors, a common type, emit a fluorescence signal upon binding with an analyte. These systems consist of two components: a fluorophore (signaling unit) and a receptor (recognition unit). Fluorescence occurs when a molecule absorbs photons

from UV-visible light, transitioning to a higher energy state, and then emits photons while returning to its ground state, though alternative de-excitation pathways also exist.[1] In 1867, F. Goppelsröder introduced the first fluorescent chemosensor, which was designed to detect aluminum ions (Al^{3+}) by forming a highly fluorescent morin chelate. This pioneering work paved the way for the creation of numerous fluorescent chemosensors for detecting various metal ions over the following decades, contributing significantly to the emergence of modern analytical chemistry.[2] Among the metal ions, zinc ion (Zn^{2+}) has garnered significant attention due to its biological importance as the second most abundant transition metal in the human body after iron. Zinc influences a variety of physiological processes, including DNA synthesis,[3] apoptosis,[4,5] gene expression,[6,7] neurotransmission[8–11] and signal transduction.[12] Additionally, Zn^{2+} modulates several ion channels[13] and serves as a crucial component in enzymes and transcription factors such as carbonic anhydrase and zinc finger proteins, where it plays both structural and catalytic roles.[14] Zn^{2+} is vital for many biological processes, including brain function, gene transcription, immune response, and reproduction,[15] and is implicated in pathological conditions such as Alzheimer's disease, epilepsy,

[a]Department of Chemistry, Christ University, Hosur Road, Bangalore, Karnataka, 560029, India. E-mail: avijitkumar.das@christuniversity.in

[b]Department of Chemistry, Prabhat Kumar College, Vidyasagar University, Purba Medinipur, W. B., 721404, India. E-mail: dolaimalay@yahoo.in

[c]Biochemistry, Molecular Endocrinology, and Reproductive Physiology Laboratory, Department of Human Physiology, Vidyasagar University, Midnapore 721102, W. B., India

[d]Department of Chemistry, Vidyasagar University, Paschim Medinipur, W. B., 721102, India

[e]Department of Applied Science, University of Quebec at Chicoutimi, Saguenay, QC, G7H 2B1, Canada

[f]Department of Mechanical Engineering, College of Engineering, King Saud University, Riyadh 11421, Saudi Arabia

ischemic stroke, and infantile diarrhea.[16] While most Zn^{2+} is tightly bound to enzymes and proteins, free zinc pools exist in tissues such as the brain, intestine, pancreas, and retina. Given its biological significance, optical imaging using fluorescent sensors for Zn^{2+} has drawn considerable interest.[17]

The design and synthesis of molecular receptors for the selective detection of biologically important Zn^{2+} ions through fluorescence changes have gained considerable attention in recent years. This is because fluorescence signals are highly sensitive to alterations in the fluorophore's surrounding environment. Due to its $3d^{10}\,4s^0$ electronic configuration, Zn^{2+} lacks intrinsic spectroscopic or magnetic properties, making it incompatible with common analytical methods like UV-vis spectroscopy, Mössbauer spectroscopy, nuclear magnetic resonance (NMR), and electron paramagnetic resonance (EPR) spectroscopy.[18] Although techniques such as atomic absorption spectroscopy offer highly accurate quantitative measurements of Zn^{2+}, they typically destroy the sample being analyzed.[19] In contrast, a fluorophore-based sensor that exhibits changes in fluorescence intensity or wavelength upon binding Zn^{2+} can provide not only the location of Zn^{2+} but also a semi-quantitative estimate in both *in vivo* and *in vitro* samples.[20] The ability of Zn^{2+} to form complexes with various organic structures that can be linked to a fluorophore makes it possible to develop fluorescent probes for biological applications.[21,22] Thus, target ligand was synthesized by normal Schiff base condensation reaction between 5-bromo-2-hydroxy-3-methoxybenzaldehyde with 3,5-dimethyl-1*H*-pyrazole-1-carbohydrazide to give the expected ligand (*E*)-*N*′-(2-hydroxy-3-methoxybenzylidene)-5-methyl-1*H*-pyrazole-3-carbohydrazide (**HMPC**) which has been shown in the Scheme 1. The target ligand **HMPC** has been characterized by ^{1}H-NMR and mass spectra (Fig. S4–S6†).

2. Experimental section

2.1 General

The chemicals and solvents were purchased from Sigma-Aldrich Chemicals Private Limited and were used without further purification. Melting points were determined on a hot-plate melting point apparatus in an open-mouth capillary and were uncorrected. ^{1}H-NMR spectra were recorded on Brucker 400 MHz instruments. NMR titration was carried out in DMSO-D_6 solvent on 400 MHz instrument with TMS as an internal standard. Chemical shifts are expressed in δ units and ^{1}H–^{1}H and ^{1}H–C coupling constants in Hz. UV-vis and fluorescence titration experiments were performed on UV-spectrophotometer: PerkinElmer, Lambda 30 and Shimadzu spectrofluorophotometer RF-6000 using a fluorescence cell of 10 mm path respectively.

2.2 Synthesis of the ligand HMPC

5-Methyl-pyrazole-3-carbohydrazide was synthesized according to reported literature method.[22] To the methanolic solution of 5-methyl-pyrazole-3-carbohydrazide (140 mg, 1.0 mmol), 5-bromo-2-hydroxy-3-methoxybenzaldehyde (152 mg, 1.0 mmol) was added and refluxed for 6 hours over oil bath (Scheme 1). The resulting solution is then concentrated to ~15 mL, cooled and a pale yellow precipitated was separated out. The yellow precipitate was filtered and washed with chilled ethanol and dried over $CaCl_2$ in a vacuum desiccator to get dry solid ligand as **HMPC**.

Yield: 150 mg, 64%. ^{1}H NMR (DMSO-d_6, 400 MHz): δ (ppm): 13.14 (s, 1H, –OH), 12.03 (s, 1H, –NH), 11.08 (s, 1H, –NH), 8.34 (s, 1H, =C–H), 7.29 (s, 1H), 7.15 (s, 1H), 6.52 (s, 1H) 3.84 (s, 3H), 2.30 (s, 3H). Mass (MS): M^+ calculated for $C_{13}H_{13}BrN_4O_3$ is 352.0171; found: 354.9801 (M + 2H$^+$).

3. Results and discussion

3.1 Binding study with Zn^{2+}

The binding study of **HMPC** ($c = 5 \times 10^{-5}$ M) with various metal ions ($c = 10^{-5}$ M) by UV-vis and fluorescence methods were carried out in an acetonitrile/aqueous (9 : 1, v/v) HEPES-buffered (1 mM, pH 7.4) solution. The UV-vis spectrum of **HMPC** showed a major absorption peak at 318 nm. Upon the gradual addition of Zn^{2+}, a gradual increase in absorbance at 318 nm was observed, indicating complexation between **HMPC** and the Zn^{2+} ion (Fig. 1). However, this absorption characteristic did not result in any visible color change.

In the fluorescence experiment, the receptor **HMPC** exhibited two emission peaks centered at 400 nm and 427 nm ($\lambda_{ex} =$ 318 nm). However, with the gradual addition of Zn^{2+} to the **HMPC** solution, a new red shifted emission peak generated at 490 nm with strong fluorescence enhancement by the appearance of naked eye blue color. As expected, **HMPC** initially
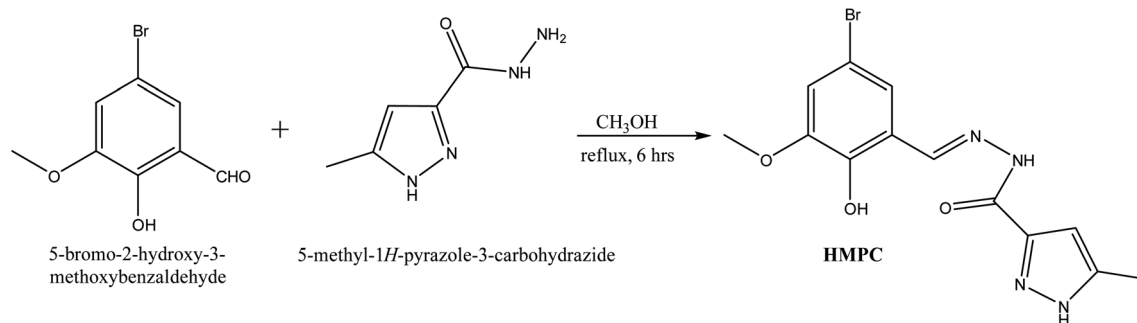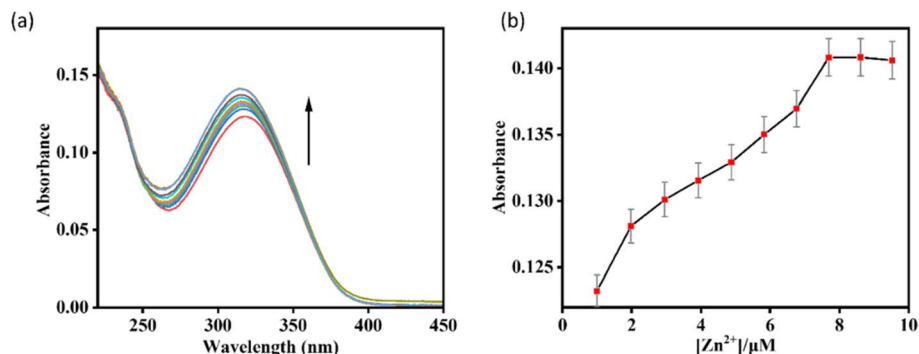

Scheme 1 Synthesis of HMPC.

Fig. 1 (a) UV-vis absorption spectra of **HMPC** ($c = 5 \times 10^{-5}$ M) in CH_3CN–HEPES buffer (9 : 1, v/v, pH = 7.4) upon addition of 0 to 5 equiv. of Zn^{2+} ($c = 10^{-5}$ M). (b) Changes of absorbance as a function of Zn^{2+} concentration including error bars (error amount, 1%; Y error bar for both [±] deviation).

exhibited weak fluorescence at 490 nm when excited at 318 nm, with a low quantum yield ($\Phi_0 = 0.1415$). Upon addition of increasing amounts of Zn^{2+}, about a 2-fold increase in fluorescence quantum yield ($\Phi/\Phi_0 = 0.259/0.142 = 2$, $\lambda_{em} = 490$ nm) was observed (Fig. 2).

One of the challenges for Zn^{2+} probes is to develop systems that are selective over a wide range of potentially competing ions, such as Mn^{2+}, Cr^{3+}, Pb^{2+}, Fe^{2+}, Co^{2+}, Ni^{2+}, Hg^{2+}, Cd^{2+}, Fe^{3+}, and Cu^{2+}. **HMPC** showed almost negligible effects on its fluorescence behavior in the presence of these competing ions, thereby maintaining its selectivity toward Zn^{2+} by naked eye as well as in the fluorescence spectra (Fig. 3).

However, Cd^{2+} exhibits slight interference because both ions share similar chemical and physical properties. Zn^{2+} and Cd^{2+} are in the same group (Group 12) of the periodic table and have comparable ionic radii, electronegativities, and coordination geometries resulting a slight interference in the fluorescence spectra of **HMPC** with Cd^{2+}. Despite this, the sensor **HMPC** demonstrated higher selectivity and sensitivity toward Zn^{2+} compared to Cd^{2+}.[23]

Competition studies were also carried out in the presence of other interfering cations to further investigate the selectivity of **HMPC** for Zn^{2+}. The fluorescence enhancement of **HMPC** for Zn^{2+} was unaffected by the presence of other interfering cations.

This indicates that the receptor **HMPC** is highly sensitive and selective for cation Zn^{2+} eventually in presence of other interfering analytes (Fig. 4). From the fluorescence titration experiments, the detection limit of **HMPC** for Zn^{2+} was calculated to be 1.68 μM using the formula $DL = K \times Sb_1/S$, where $K = 3$, Sb_1 is the standard deviation of the blank solution, and S is the slope of the calibration curve, (Fig. S2†).[24] Job plot analysis indicated 1 : 1 binding stoichiometry between **HMPC** with Zn^{2+} (Fig. S3†) and from the fluorescence titration experiment, the association constant (K_a) of **HMPC** with Zn^{2+} was calculated as 5×10^4 M^{-1} (error < 10%) (Fig. S1†).[25]

The reversible binding of **HMPC** with the metal ion Zn^{2+} has been proved by the reversibility experiment carried out by adding an aqueous solution of excess Na_2EDTA (0–5.0 equiv.) *in situ* to the solution of **HMPC-Zn^{2+}** complex (Fig. 5). And it has been observed that the fluorescence intensity of **HMPC-Zn^{2+}** complex is quenched steadily in presence of excess Na_2EDTA which indicates that Na_2EDTA possibly strips away Zn^{2+} from the metal binding cavity.

3.2 Probable binding mode in solution phase

Probable binding of **HMPC** with Zn^{2+} was demonstrated by UV-vis, fluorescence and mass spectrometry. Initially **HMPC** alone
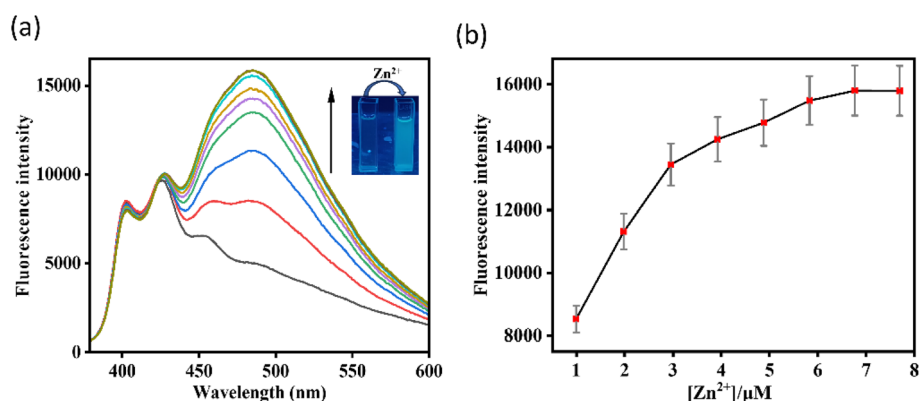

Fig. 2 (a) Fluorescence spectra of **HMPC** ($c = 5 \times 10^{-5}$ M) in CH_3CN–HEPES buffer (9 : 1, v/v, pH = 7.4) upon addition of 0 to 5 equiv. of Zn^{2+} ($c = 10^{-5}$ M). Inset: changes of emission color on addition of Zn^{2+} ions (b) changes of emission intensity of **HMPC** as a function of Zn^{2+} concentration including error bars (error amount, 5%; Y error bar for both [±] deviation).
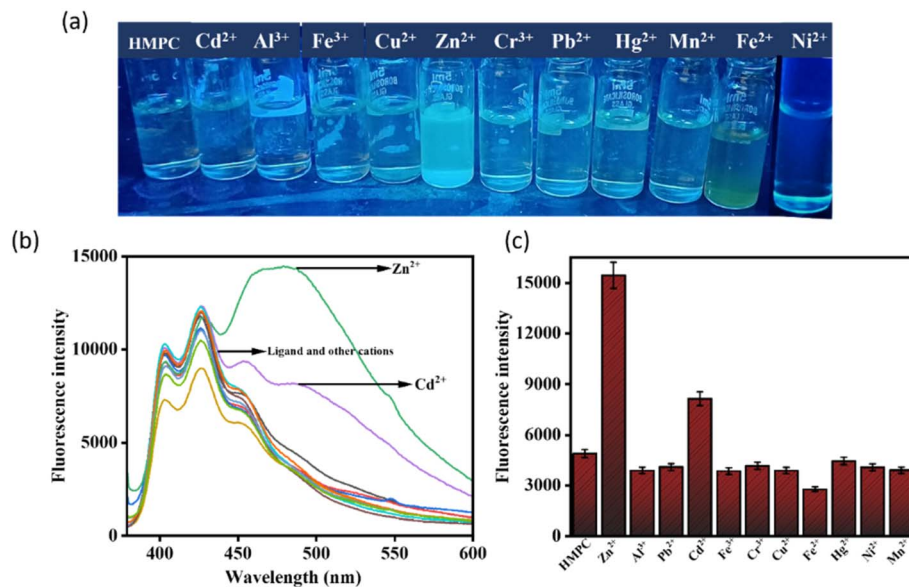
Fig. 3 (a) Fluorescence color changes of **HMPC** in presence of various cations. (b) Fluorescence titration spectra of **HMPC** ($c = 5 \times 10^{-5}$ M) in HEPES buffered aqueous CH_3CN (9 : 1, v/v) upon addition of 15 equiv. of different metal ions. (c) A comparative fluorescence response of **HMPC** by bar representation in presence of different cations.
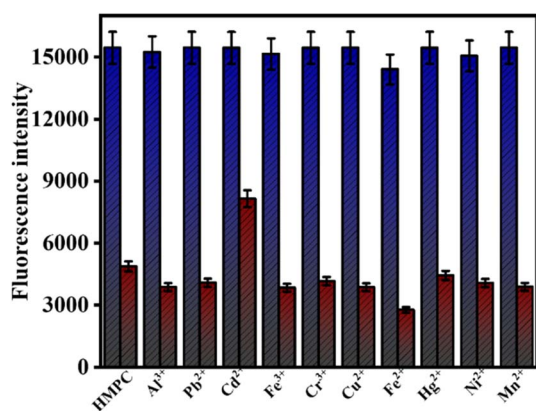

Fig. 4 (Maroon bars) variation of fluorescence intensity of **HMPC** + 15 equiv. M^{n+}; (blue bars) fluorescence intensity of **HMPC** + 15 equiv. M^{n+}, followed by 10 equiv. Zn^{2+}.

showed weak fluorescence exhibiting two emission signals at 400 nm and 427 nm but in the presence of Zn^{2+}, a notable red shifted fluorescence enhancement was observed at 490 nm. This remarkable fluorescence enhancement of **HMPC** in presence of Zn^{2+} can be attributed due to the suppression of PET process within the molecule and enhancement of ICT for the charge transfer between ligand and metal, which results also generation of the fluorescence enhancement by chelation enhanced fluorescence (CHEF) mechanism. Before binding with Zn^{2+} (off-state), the fluorescence of free **HMPC** is very weak due to operating PET from electron donor phenolic hydroxy group to electron acceptor hydrazide coupled imine moiety and weak ICT (Scheme 2). In the presence of Zn^{2+}, the ligand **HMPC** forms four coordination *via* the bond formation between O_2 donors from hydroxy and hydrazide moieties and one nitrogen

from imine nitrogen and one negative chloride counter anion resulting in fluorescence enhancement (on-state) by CHEF.[26] On the other hand, the emission intensity of **HMPC** is notably very weak due to the radiationless deactivation of the excited state caused by conformational changes *via* the free rotation around the imine (C=N) bond, a phenomenon commonly observed in Schiff-base dyes. But, co-ordination with Zn^{2+} inhibits the isomerization which results the increase of fluorescence intensity of the ligand for enhanced ICT.[27] The formation of a complex between **HMPC** and Zn^{2+} has been verified through the emergence of a mass peak at $m/z = 450.6280$, attributed to $[\textbf{HMPC} + Zn^{2+} + Cl^-]$ (Fig. S6† and Scheme 2), which has been justified also by 1 : 1 binding stoichiometric ratio in the Jobs plot analysis and theoretical calculation.

3.3 DFT study

The optimized geometry of **HMPC** and **HMPC** + Zn^{2+} complex through DFT is shown in Fig. 6. The **HMPC** + Zn^{2+} complex having metal centre Zn^{2+} are tetra-coordinated with neutral ligand with O_2 donor system, one nitrogen and one negative chlorides counter anion, satisfy the tetrahedral geometry to form the mononuclear complex. The theoretical Zn–Cl and Zn–N (of imine) bond distances are as 2.175 Å and 2.003 Å respectively and Zn–O bond lengths are 2.199 Å (amide oxygen) and 1.947 Å (phenolic oxygen) for **HMPC** + Zn^{2+} complex. Moreover, it is found that the HOMO–LUMO energy gap are $\Delta E = 7.652$ eV and 6.984 eV for **HMPC** and **HMPC** + Zn^{2+} complex respectively which is responsible for the stabilization of the complex formation (Fig. 7).

Experimental absorbance of ligand **HMPC** at 328 nm at room temperature was increased by the gradual addition of Zn^{2+}. The theoretical electronic spectra shows the corresponding
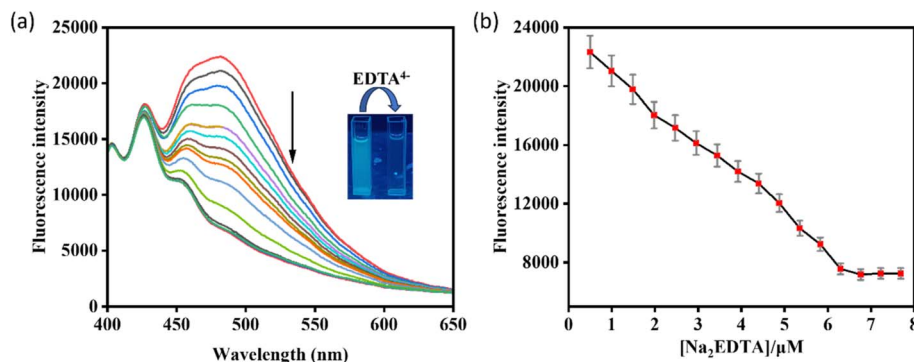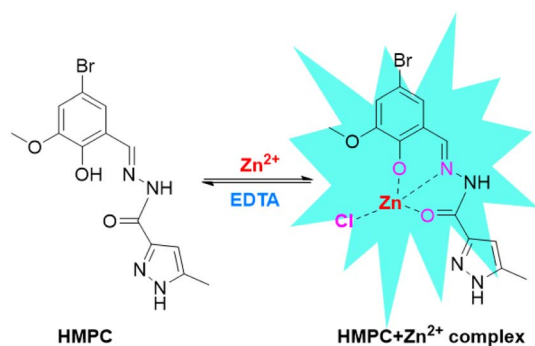
Fig. 5 (a) Fluorescence titration spectra of **HMPC-Zn^{2+}** complex ($c = 5 \times 10^{-5}$ M) with Na$_2$EDTA (0–5.0 equiv.) in CH$_3$CN−HEPES buffer (9 : 1, v/v, pH = 7.4). Inset: bluish white colored emission observed with Zn^{2+} was disappeared in presence of Na$_2$EDTA. (b) Change of emission intensity as a function of Na$_2$EDTA concentration including error bars (error amount, 5%; Y error bar for both [±] deviation.
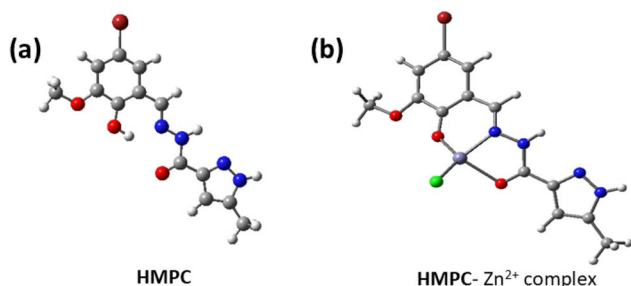

Scheme 2 Probable binding mode in solution phase.

Fig. 6 Geometry optimized molecular structure of (a) **HMPC** and (b) **HMPC-Zn^{2+}** complex.

Fig. 7 Frontier molecular orbital with energy difference of **HMPC** and complex.

calculated absorption band at 317 nm, demonstrating excellent agreement with the experimental data and these spectral bands can be attributed to the S$_0$ → S$_7$ transition.

3.4 Biological application

MCF-7 cells at sub-confluent volume were cultured in DMEM for 24 hours under standard conditions in a CO$_2$ incubator. Following this, **HMPC** was administered to the cells at its determined IC$_{50}$ concentration. After an appropriate incubation period, fluorescence images of the treated MCF-7 cells were captured at 40× magnification using a ZEISS fluorescence microscope (Germany). In parallel, the cells were also exposed
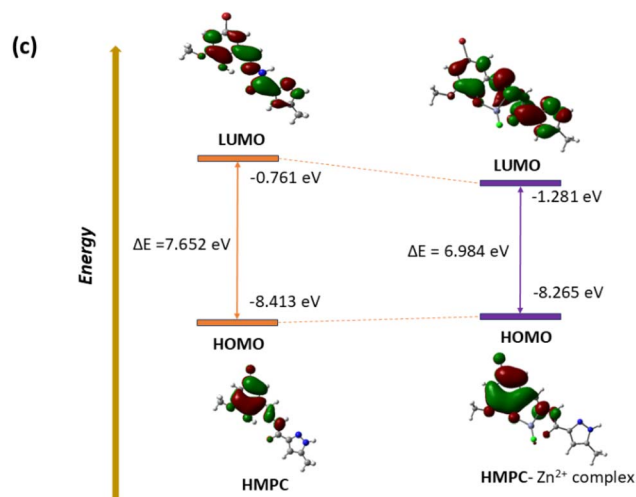
to a 10 μM Zn^{2+} solution for one hour, and additional fluorescence images were captured at excitation wavelengths of 582 nm and 581 nm for the cells pre-treated with **HMPC** at the IC$_{50}$ concentration, as described by Mabhai et al. (2019).[28]

3.4.1 Cell viability study on MCF 7 and human lymphocyte cells (HLCs). The cytotoxic effects of **HMPC** on MCF-7 and HCT-116 cells were assessed using the MTT assay, which revealed a significant dose-dependent reduction in cell viability, indicating potent cytotoxicity. The IC$_{50}$ value of **HMPC** was found to be 19.26 μg mL^{-1} for MCF-7 cells and 21.31% μg mL^{-1} for HCT-116 cells, which are comparable to the IC$_{50}$ of the standard anticancer drug 5-FU (16.14 μg mL^{-1} for MCF-7 and 10.21 μg mL^{-1} for HCT-116). These results further substantiate the potent cytotoxic activity of **HMPC** (Fig. 8A and B). A time-dependent study demonstrated that **HMPC** treatment resulted in a 48.47% reduction in cell viability for MCF-7 cells and a 51.49% reduction for HCT-116 cells at 24 hours. At 48 hours, the reduction in cell viability was 30.89% for MCF-7 cells and 38.23% for HCT-116 cells (Fig. 8C). These results underscore the strong cytotoxic potential of **HMPC** against MCF-7 and HCT-116
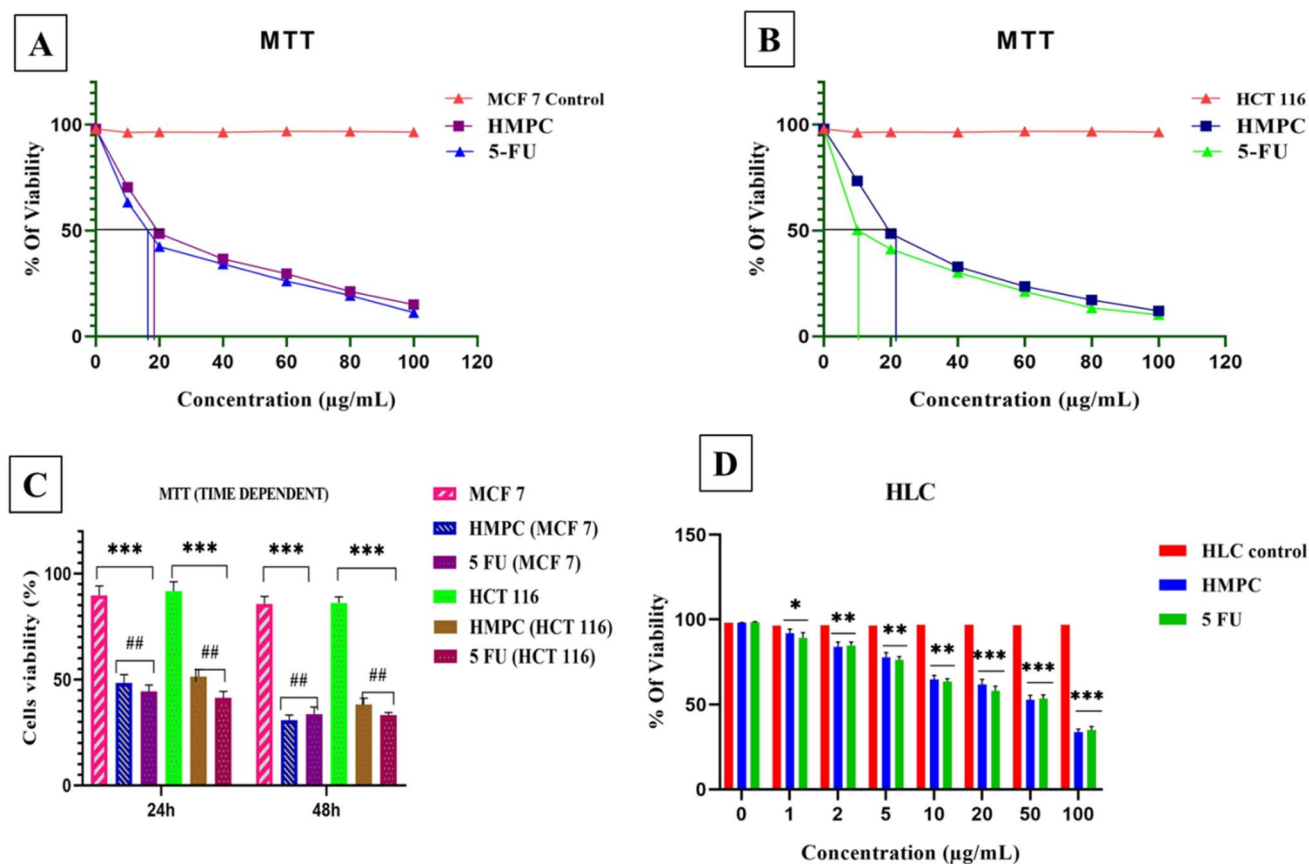
Fig. 8 MTT assay: cytotoxic effects of HMPC on MCF-7 cells at different concentrations, with an IC_{50} value of 19.26 μg mL^{-1} (A). Cytotoxic effects of HMPC on HCT-116 cells at different concentrations, with an IC_{50} value of 21.31 μg mL^{-1} (B). Cell viability was assessed at 24 h and 48 h following treatment with HMPC at its IC_{50} concentrations (C). Cytotoxic study on HLC: a slight decrease in lymphocyte viability was observed at much higher concentration of HMPC (50 μg mL^{-1}) (D). Data are presented as mean ± SEM of three independent experiments; **$p < 0.01$, ***$p < 0.001$, compared to the control group.

cell lines. Furthermore, HMPC exhibited minimal toxicity to human lymphocytes at concentrations up to 50 μg mL^{-1}, with a slight reduction in cell viability, as the viability at 50 μg mL^{-1} was recorded at 52.32%. Overall, these findings suggest that HMPC could be a promising anticancer agent for targeting MCF-7 and HCT-116 cells (Fig. 8D, HLC).
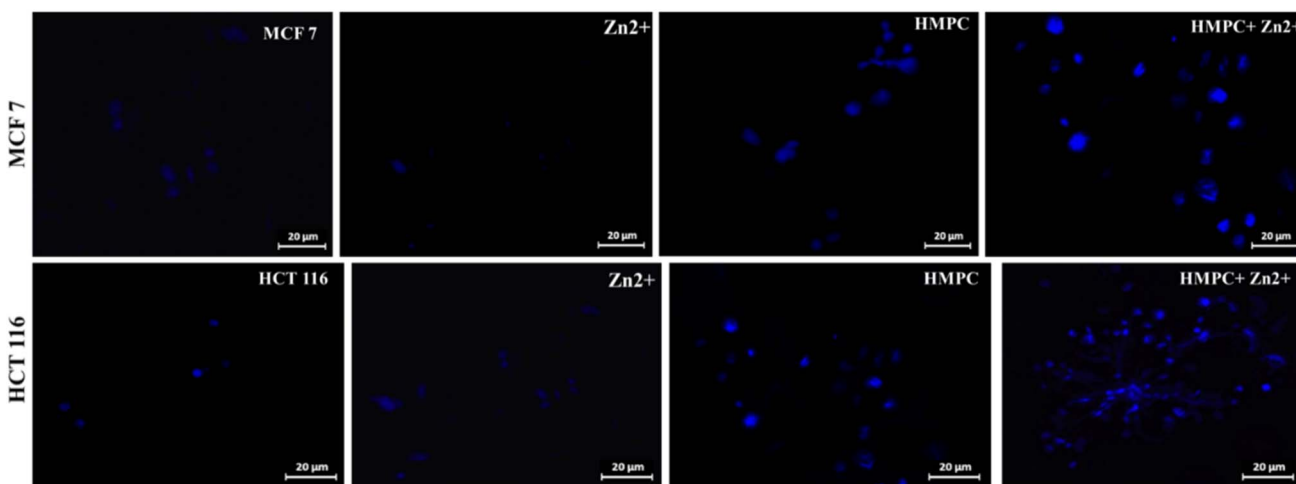

Fig. 9 Intercellular biosensor cell imaging study was investigated on MCF 7 and HCT 116 cells. Cells were incubated alone with free HMPC and brighter blue fluorescence was observed HMPC-Zn^{2+} treated groups other than HMPC. The image was captured by a fluorescence microscope (ZEISS, Germany).

Table 1 Results of the docking of ligands and target protein 2VCJ

Name of ligands	Docking score (kcal mol^{-1})
HMPC	-7.1

Table 2 Results of the docking of ligands and target protein 1T69

Name of ligands	Docking score (kcal mol^{-1})
HMPC	-6.5

3.4.2 Fluorescence cell imaging study. During 1 hour incubation at 37 °C with **HMPC** at its IC$_{50}$ concentration, less significant intracellular fluorescence was observed in fluorescent cell imaging on MCF-7 and HCT-116 cell lines. However, when the cells were incubated with an exogenous Zn^{2+} ion solution, a strong intracellular blue fluorescence was detected, with the fluorescence intensity of the **HMPC-Zn^{2+}** + complex being significantly higher (Fig. 9). This indicates that **HMPC** effectively penetrates the cell membrane and binds to intracellular Zn^{2+} ions, forming the **HMPC-Zn^{2+}** complex, as demonstrated by the fluorescence imaging. The fluorescence generation mechanisms of **HMPC**, Density Functional Theory (DFT) calculations were employed to analyze the electronic structure and frontier molecular orbitals of **HMPC** and the **HMPC-Zn^{2+}** complex. The results suggest that the fluorescence arises from the ligand-to-metal charge transfer mechanism facilitated by the coordination of Zn^{2+} ions with the **HMPC** molecule. In its free state, **HMPC** exhibits a less efficient intramolecular charge transfer due to the absence of metal ion coordination, which explains the low fluorescence intensity observed. Upon binding with Zn^{2+}, the electronic transitions are significantly altered, as evidenced by leading to enhanced fluorescence.

The strong blue fluorescence of the **HMPC-Zn^{2+}** complex highlights the specificity and efficiency of the Zn^{2+} binding. These findings demonstrate that **HMPC** could serve as a selective sensor for Zn^{2+} ions in bio-imaging applications under the given concentrations and incubation conditions, without inducing cytotoxic effects. By combining experimental fluorescence imaging and computational analysis, we provide a comprehensive understanding of **HMPC** have potential as a Zn^{2+} ion sensor against MCF-7 and HCT-116 cells.

3.5 Molecular docking study

The link between the mark protein (PDB-ID: 2VCJ) and the ligands is assessed by molecular docking.[28–34] The designs reveal the free energy change of ligand **HMPC** for the interactions with protein 2VCJ, $\Delta G = -7.1$ kcal mol^{-1} (Table 1) inside a grid box of $28.6 \times 12.7 \times 19.82$ Å with dimensions $25 \times 25 \times 25$ Å along three axes (Fig. 10a). The 2D diagram shows that ligand **HMPC** forms one hydrogen bonding interaction with the 51st asparagine residue, along with a pi–sulfur bond with the 98th methionine residue of the A chain in the binding site of the protein 2VCJ (Fig. 10b).

The link between the mark protein (PDB-ID: 1T69) and the ligand **HMPC** is assessed by molecular docking. The designs reveal the free energy change of ligand **HMPC** for the interaction with protein 1T69, $\Delta G = -6.5$ kcal mol^{-1} (Table 2) inside a grid box of $30.09 \times -3.16 \times -13.64$ Å with dimensions $22 \times 22 \times 22$ Å along three axes (Fig. 11a). The 2D diagram (Fig. 11b) shows that ligand **HMPC** forms two hydrogen bonding interactions with the 33rd lysine residue and 180th histidine residue of chain A in the binding site of the protein 1T69, along with van der Waals and pi–pi stacked interactions as shown in the Fig. 11b.

3.6 ADME prediction results

The result from SWISS-ADME[35] is agreeable as **HMPC** offers no violation of Lipinski's, Veber's, and Egan's rule of drug-likeness properties and it has high gastrointestinal absorption
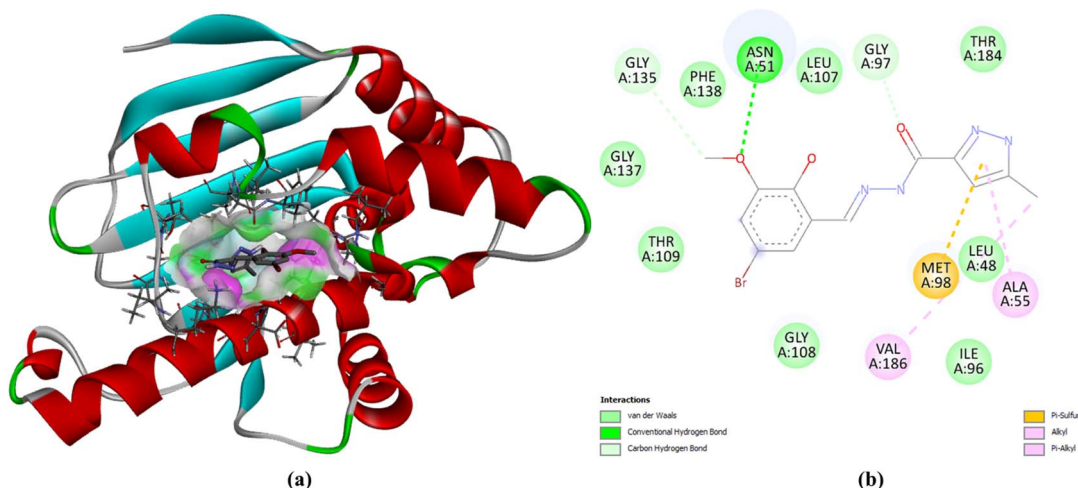

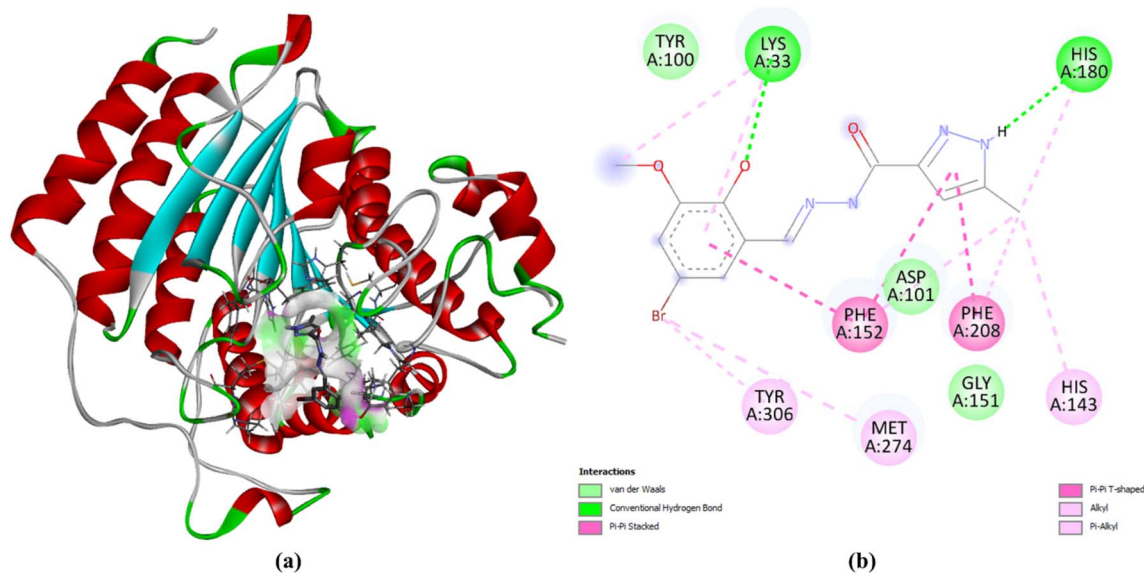Fig. 10 Docking poses of **HMPC** with 2VCJ, (a) at active site, (b) 2D diagram of the docked complex.

Fig. 11 Docking poses of **HMPC** with 1T69, (a) at active site, (b) 2D diagram of the docked complex.

(Fig. S7a†), no blood–brain barrier (BBB) permeant property (Fig. S7a†), it has a good bio-radar (Fig. S7b†) which makes it orally admissible to people. **HMPC** does not inhibit any of the cytochrome P50 enzymes except the CYP1A2 inhibitor, and is not a *P*-gp substrate. It has a good log *P* value of 1.97, essential for showing drug-like properties. It has a Total Polar Surface Area (TPSA) of 99.60 Å^2 (Table S1†).

4. Conclusion

In conclusion, the fluorescent sensor **HMPC** has demonstrated high selectivity and sensitivity for Zn^{2+} detection, with a detection limit well below the WHO guideline. Its fluorescence enhancement is driven by a CHEF mechanism through the suppression of PET and enhancement of ICT, as validated by comprehensive spectroscopic analyses and computational studies. Additionally, **HMPC** shows promising biological applications, including low cytotoxicity and potential anti-cancer activity, as supported by molecular docking studies with HSP90 and HDAC8 proteins. With a favorable ADME profile and strong binding affinities, **HMPC** presents potential not only as a fluorescent probe for Zn^{2+} but also as a candidate for anti-cancer drug development. Furthermore, the cytotoxicity and cell imaging studies conducted with MCF-7 cells indicate the potential of **HMPC** for biological applications, paving the way for further exploration in the field of chemosensing and biomedicine.

Data availability

The data supporting this article have been included as part of the ESI.†

Conflicts of interest

The authors declare no competing financial interest.

Acknowledgements

References

1 A. W. Czarnik, *Acc. Chem. Res.*, 1994, **27**, 302–308.

2 A. W. Czarnik, *J. Org. Chem.*, 1993, **58**, 5797–5801.

3 J. Fraústo da Silva and R. J. P. Williams, in *The Biological Chemistry of the Elements*, Clarendon Press, Oxford, 1991, p. 302.

4 P. D. Zalewski, I. J. Forbes, G. Mazdai and C. Giannakis, *Biochem. Inter.*, 1991, **24**, 1093–1101.

5 S. J. Martin, G. Mazdai, J. J. Strain, T. G. Cotter and B. M. Hannigan, *Clin. Exp. Immunol.*, 1991, **83**, 338–344.

6 D. E. Epner and H. R. Herschman, *J. Cell. Physiol.*, 1991, **148**, 68–74.

7 R. J. Cousins and L. M. Lee-Ambrose, *J. Nutr.*, 1992, **122**, 56–64.

8 X. M. Xie and T. G. Smart, *Nature*, 1991, **349**, 521–524.

9 C. J. Frederickson, *Int. Rev. Neurobiol.*, 1989, **31**, 145–238.

10 L. M. T. Canzoniero, S. L. Sensi and D. W. Choi, *Neurobiol. Dis.*, 1997, **4**, 275–279.

11 D. W. Choi and J. Y. Koh, *Annu. Rev. Neurosci.*, 1998, **21**, 347–375.

12 F. Grummt, C. Wienmann-Dorsch, J. Schneider-Schaulies and A. Lux, *Exp. Cell Res.*, 1986, **163**, 191–200.

13 N. L. Harrison and S. Gibbons, *J. Neuropharmacology*, 1994, **33**, 935–952.

14 B. L. Vallee and K. H. Falchuk, *Physiol. Rev.*, 1993, **73**, 79–118.

15 (*a*) C. J. Frederickson, J.-Y. Koh and A. I. Bush, *Nat. Rev. Neurosci.*, 2005, **6**, 449; (*b*) S. Goswami, S. Maity, A. C. Maity, A. K. Das, K. Khanra, T. K. Mandal and N. Bhattacharyya, *Tetrahedron Lett.*, 2014, **55**, 5993–5997; (*c*) S. Maity, A. C. Maity, A. K. Das and N. Bhattacharyya, *Anal. Methods*, 2022, **14**, 2739–2744.

16 (*a*) A. I. Bush, W. H. Pettingell, G. Multhaup, M. d Paradis, J. P. Vonsattel, J. F. Gusella, K. Beyreuther, C. L. Masters and R. E. Tanzi, *Science*, 1994, **265**, 1464–1467; (*b*) F. Joy, K. P. Chaithra, A. Nizam, A. Deepti, P. S. Baby Chakrapani, A. K. Das, T. P. Vinod and Y. Nair, *Chem. Eng. J.*, 2023, **453**, 139798; (*c*) G. C. Das, A. Kumar Das, D. Das, T. Raj Maity, A. Samanta, F. Ali Alasmary, A. Salem Almalki, A. Iqbal and M. Dolai, *J. Photochem. Photobiol., A*, 2023, **440**, 114663.

17 (*a*) Z. Xu, J. Yoon and D. R. Spring, *Chem. Soc. Rev.*, 2010, **39**, 1996–2006; (*b*) S. Goswami, A. K. Das, K. Aich, A. Manna, S. Maity, K. Khanra and N. Bhattacharyya, *Analyst*, 2013, **138**, 4593–4598.

18 P. Jiang and Z. Guo, *Coord. Chem. Rev.*, 2004, **248**, 205–229.

19 (*a*) D. A. Skoog, F. James Holler and S. R. Crouch, *Principles of Instrumental Analysis*, Cengage Learning, 2017, vol. 27, pp. 992; (*b*) S. Sogra, V. Aishwarya, P. S. Chaithra, L. Suchi, S. Abhishek, S. Vishnu and A. K. Das, *J. Fluoresc.*, 2024, DOI: 10.1007/s10895-023-03552-1; (*c*) A. K. Das and S. Goswami, *Sens. Actuators, B*, 2017, **245**, 1062–1125; (*d*) R. Pandey, A. Kumar, Q. Xu and D. S. Pandey, *Dalton Trans.*, 2020, **49**, 542–568.

20 W.-K. Dong, S. Folaranmi Akogun, Y. Zhang, Y.-X. Sun and X.-Y. Dong, *Sens. Actuators, B*, 2017, **238**, 723–734.

21 Q.-Y. Yu, C.-W. Wei, X.-J. Wang, S.-Q. Gao, X.-Y. Tong and Y.-W. Lin, *J. Biol. Inorg. Chem.*, 2023, **28**, 205–211.

22 (*a*) P. Bera, N. Saha, S. Kumar, D. Banerjee and R. Bhattacharya, *Transition Met. Chem.*, 1999, **24**, 425; (*b*) B. Das, K. Chandra Murmu, S. K. Dey, S. M. Chaudhuri, Z. M. Almarhoon, M. Z. Ansari, P. P. Bag and M. Dolai, *Inorg. Chem. Commun.*, 2024, **170**, 113108; (*c*) S. Goswami, S. Maity, A. C. Maity, A. K. Das, K. Khanra, T. K. Mandal and N. Bhattacharyya, *Tetrahedron Lett.*, 2014, **55**, 5993–5997; (*d*) S. Goswami, A. K. Das, B. Pakhira, S. B. Roy, A. K. Maity, P. Saha and S. Sarkar, *Dalton Trans.*, 2014, **43**, 12689–12697.

23 (*a*) K. Komatsu, K. Kikuchi, H. Kojima, Y. Urano and T. Nagano, *J. Am. Chem. Soc.*, 2005, **127**, 10197–10204; (*b*) H. H. Wang, Q. Gan, X. J. Wang, L. Xue, S. H. Liu and H. Jiang, *Org. Lett.*, 2007, **9**, 4995–4998; (*c*) J. Du, J. Fan, X. Peng, H. Li and S. Sun, *Sens. Actuators, B*, 2010, **144**, 337–341.

24 M. Shortreed, R. Kopelman, M. Kuhn and B. Hoyland, *Anal. Chem.*, 1996, **68**, 1414–1418.

25 (*a*) H. A. Benesi and J. H. Hildebrand, *J. Am. Chem. Soc.*, 1949, **71**, 2703–2707; (*b*) Y. Shiraishi, Y. Kohno and T. Hirai, *Ind. Eng. Chem. Res.*, 2005, **44**, 847–851.

26 H. Niu, J. Liu, H. M. O'Connor, T. Gunnlaugsson, T. D. James and H. Zhang, *Chem. Soc. Rev.*, 2023, **52**, 2322–2357.

27 (*a*) M. A. Haidekker and E. A. Theodorakis, *Org. Biomol. Chem.*, 2007, **5**, 1669–1678; (*b*) A. K. Chibisov, G. V. Zakharova and H. Görner, *J. Chem. Soc., Faraday Trans.*, 1996, **92**, 4917–4925; (*c*) M. S. A. Abdel-Mottaleb, R. O. Loutfy and R. Lapouyade, *J. Photochem. Photobiol., A*, 1989, **48**, 87–93; (*d*) M. S. Kumar, V. S., M. Dolai, A. Nag, Y. Bylappa and A. K. Das, *Anal. Methods*, 2024, **16**, 676–685.

28 (*a*) S. Pakrashy, P. K. Mandal, J. Nanda Goswami, S. K. Dey, S. Maiti Choudhury, B. Bhattacharya, F. Emmerling, F. A. Alasmary and M. Dolai, *ACS Omega*, 2022, **7**, 48572–48582; (*b*) S. Mabhai, M. Dolai, S. K. Dey, A. Dhara, S. M. Choudhury, B. Das, S. Dey and A. Jan, *Spectrochim. Acta, Part A*, 2019, **219**, 319–332.

29 S. Pakrashy, P. K. Mandal, S. K. Dey, S. M. Choudhury, F. A. Alasmary, A. S. Almalki, M. A. Islam and M. Dolai, *ACS Omega*, 2022, **7**, 33408–33422.

30 S. Misra, S. Pakrashy, S. Paul, P. K. Maurya, P. S. Sardar, A. Bose and A. Majhi, Interaction of a new triazole compound with Serum albumins and Proteolytic enzyme Bromelain by Steady state fluorescence and Molecular docking techniques, *J. Biochem., Mol. Biol. Biophys.*, 2024, **61**, 305–313.

31 S. Misra, S. Paul, S. Pakrashy, S. Ghosh, S. Naskar, P. K. Maurya, P. S. Sardar, K. Venkateswarlu, A. Bose and A. Majhi, *Indian J. Chem.*, 2023, **62**, 1001–1011.

32 M. Dolai, S. Pakrashy, A. K. Ghosh, S. Biswas, S. Konar, F. A. Alasmary, A. S. Almalki and M. A. Islam, *J. Mol. Struct.*, 2023, **1274**, 134584.

33 B. Das, S. Pakrashy, G. C. Das, U. Das, F. A. Alasmary, S. M. Wabaidur, M. A. Islam and M. Dolai, *J. Fluoresc.*, 2022, **32**, 1263–1277.

34 S. Pakrashy, S. Chakraborty, S. Manna, J. Nanda Goswami, B. Bhattacharya, F. Emmerling, J. Mandal, S. Misra, S. Maiti Choudhury, M. K. Okla, A. Bose, P. K. Maurya, A. Majhi and M. Dolai, *ACS Appl. Bio. Mater.*, 2024, **7**, 3414–3430.

35 A. Daina, O. Michielin and V. Zoete, *Sci. Rep.*, 2017, **7**, 42717.